Application of Adaptive Parallel Fast Marching Method in Automatic Submarine Cable Path Planning

Xinyu Wang, Zengfu Wang and Moshe Zukerman, *Life Fellow, IEEE*

***Abstract*—Submarine optical fiber communication cables (subsequently referred to as submarine cables) form the backbone of the Internet's infrastructure. Damage to these cables can precipitate Internet outages with far-reaching socio-economic impacts. The prevailing practice of manual cable routing is laborious, considering the thousands of kilometers these cables span. It also fails to strike an optimal balance between cost and risk due to its lack of scalability and precision. The Fast Marching Method (FMM), a non-iterative, precise numerical approach capable of solving the Eikonal equation, offers a viable alternative by optimizing the required path between source and destination, considering a summary objective function of costs and risk factors. An interpretation of its solution signifies the optimum value of the objective function between a starting point and all other points. However, the sequential nature of the FMM algorithm suffers from computational limitations and impedes direct parallelization. In this study, we introduce an Adaptive Parallel FMM (APFMM), an innovative approach utilizing adaptive domain decomposition and dynamic multi-resolution analysis. This scalable and widely applicable method can overcome the limitations of existing methods and achieve planning of high-precision, ultra-long-distance (over 14,000 km) submarine cable routes over the Earth's surface. Simulated experiment results corroborate that APFMM effectively overcomes the computational challenges posed by the sequential FMM when dealing with large datasets. Additionally, it reduces the running time by more than 81% compared to the traditional parallel FMM. This marks a substantial advancement in facilitating efficient, automated, high-precision planning for long-distance submarine cable paths.**

***Note to Practitioners*—This paper introduces APFMM, a novel technique based on adaptive domain decomposition and multi-resolution analysis, facilitating high-precision, ultra-long-distance (over 14,000 km) submarine cable path planning. Results from simulated experiments show that APFMM not only overcomes the computational constraints associated with the sequential FMM for large datasets but also cuts the running time by more than 81% relative to the conventional parallel FMM.**

This breakthrough improvement holds significant implications for practitioners in submarine cable design and construction. With the use of APFMM, designers can plan and optimize cable paths more efficiently, thereby lowering cabling costs and enhancing network resilience. Furthermore, the application of APFMM is not limited to submarine cable path planning and can be employed in other domains involving large-scale data processing and complex path planning, such as electricity cables, gas pipelines, and transportation route planning. While our focus in this paper is primarily on submarine cable path planning, we anticipate practitioners extending the application of APFMM to other use cases, realizing broader utility and benefits.

***Index Terms*—Submarine optical fiber cables, path planning, adaptive parallel FMM, domain decomposition methods, multi-resolution method, cost-effectiveness, survivability.**

I. Introduction

SUBMARINE optical fiber communication cables (hereafter submarine cables) are crucial for our interconnected world, carrying over 99% of global voice and data traffic [1]. With 600 active and planned systems spanning 1.4 million kilometers and costing around 25,000 USD per kilometer as of June 2024 [2], these cables are vital for the global digital infrastructure. In 2023, the submarine cable systems market was valued at USD 14.2 billion. It is forecasted to grow at a compound annual growth rate of over 9.5% from 2024 to 2032 [3]. This growth is supported by strategic initiatives like China's "One Belt One Road" [4] and significant investments from tech giants like Google, Amazon, Meta, and Microsoft [5]. See the submarine cable world map in Fig. 1.

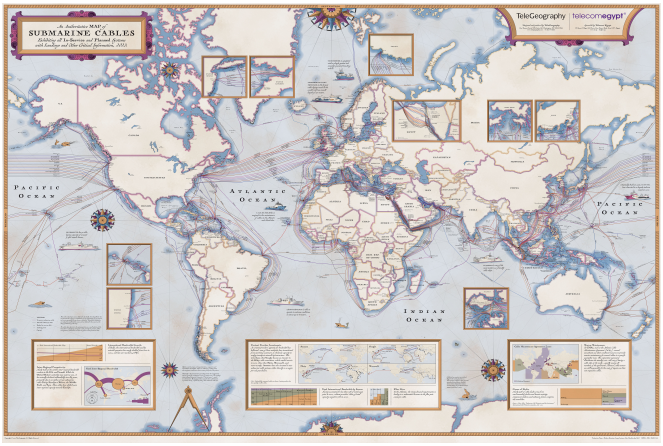

Fig. 1: Global communications are facilitated by the use of submarine cables. Source: TeleGeography.

While the costs of laying and maintaining submarine cables are high, this essential infrastructure is also vulnerable to

This work was in part supported by the Hong Kong Innovation and Technology Commission (InnoHK Project CIMDA) and by a grant from the Research Grants Council of the Hong Kong Special Administrative Region, China (CityU 11201922). *(Corresponding author: Zengfu Wang.)*

Xinyu Wang is with the Center for Intelligent Multidimensional Data Analysis, Hong Kong SAR, China. (email: xywang47-c@my.cityu.edu.hk).

Moshe Zukerman is with the Department of Electrical Engineering, City University of Hong Kong, Kowloon, Hong Kong SAR, China. (e-mail: m.zu@cityu.edu.hk).

Zengfu Wang is with the Research & Development Institute of Northwestern Polytechnical University in Shenzhen, Shenzhen 518057, China, and also with the School of Automation, Northwestern Polytechnical University, Xi'an 710072, China. (e-mail: wangzengfu@nwpu.edu.cn).

natural and anthropogenic hazards [6], with over 100 faults reported annually [2]. Events like the 2006 Hengchun earthquake [7] and the 2022 undersea volcano eruption disrupting the Tonga-Fiji cable system [8] illustrate the risks of considerable disruptions to global communication networks. Such incidents can have profound socio-economic impacts, especially in sectors like finance, where brief interruptions can cause substantial losses.

In light of the absence of automated submarine cable path planning, industry practices primarily depend on manual methods and expert judgment. This manual approach utilizes a range of data and tools to propose and evaluate potential paths. However, this subjective process not only typically spans several months or even years but also may fail to ensure the most optimal cable routes. Motivated by these challenges, this study endeavors to design and implement a novel methodology that delivers optimal path-planning solutions based on comprehensive data considerations. This approach facilitates efficient, automated, and high-precision long-distance submarine cable path planning. The implications of this method are significant for practitioners cause it enables designers to more effectively plan and optimize cable paths, thereby reducing cabling costs and enhancing the resilience of network infrastructure.

The Fast Marching Method (FMM) [9], an asymptotically optimal numerical method for solving the Eikonal equation, has proven to be highly effective. It is now broadly applied to identify optimal paths in a variety of scenarios [10–15]. The solution of FMM can be interpreted as the *shortest* or *least-cost* path from a given starting point to all other points over a triangulated manifold that models the Earth's surface [9]. FMM operates based on an ordered heap algorithm, starting at the source point and "marching" outward. At each step, it selects the unprocessed grid point (or pixel) with the shortest total travel time (the least life-cycle cost in this context) and updates the travel times of its neighbors. This process continues until all points are processed or the destination is reached. Finally, the least life-cycle cost path from the destination to the source can be found by backtracking along the gradient of the travel time. In the context of submarine cable path planning, we refer to "cost" as "life-cycle cost", where the life-cycle cost of submarine cables is the total cost over their entire life span, typically 25 years [2]. During this period, the path of the submarine cable remains static unless exceptional circumstances, such as irreparable damage from geological disasters or human activities, necessitate a change. Life-cycle cost covers a variety of factors that affect the construction, maintenance, and repair of submarine cables, such as cable length, earthquakes, volcanic eruptions, seabed slope, water depth, sediment hardness, marine protected areas, and human-related activities (fishing and anchoring), and so on [16].

The demand for ultra-long distance (over 10,000 km) interoceanic cables is on the rise, driven by the evolving needs of global communication [2]. The design of high-precision, transoceanic submarine cable paths across vast areas poses significant challenges, particularly due to the sequential characteristics of the FMM. In this context, we refer to the traditional FMM, which does not employ any parallelization techniques, as Sequential FMM (SFMM), and the version that utilizes parallelization technologies as Parallel FMM (PFMM). SFMM struggles with handling the large data volumes required for path planning within an extensive target area where the data resolution is high, often resulting in prohibitively long computation times. In some cases, the data volume is so substantial that direct computation becomes practically unfeasible. This situation is particularly problematic for large-scale projects and brings us to a critical research question: How can we develop faster and more efficient algorithms that meet the computational demands of large-scale, ultra-long-distance submarine cable path planning within reasonable timeframes and with manageable resource use? This question underscores the need for innovative algorithms to overcome the challenge of handling extensive computational tasks in ultra-long-haul and high-precision submarine cable path planning.

In this paper, we introduce a new method, which we call *Adaptive Parallel FMM* (APFMM), a sophisticated algorithm specifically developed for high-precision and ultra-long-distance submarine cable path planning. This innovative algorithm tackles the computational challenges in vast target areas, boosts operational efficiency, and enhances solution accuracy. By integrating the Domain Decomposition Method (DDM) with Multi-Resolution Analysis (MRA), our APFMM achieves optimized thread load balancing and reduces communication overhead among adjacent sub-domains. Importantly, our APFMM does not merely apply existing DDM and MRA methodologies to the task of submarine cable path planning. Instead, it innovatively combines DDM with MRA dynamically for the first time, marking a significant advancement in this field. This unique combination significantly enhances computational efficiency, surpassing traditional SFMM and static domain decomposition-based PFMMs in the existing literature. The advancements presented by our APFMM are particularly vital in an industry where traditional manual, expert-driven design processes are both time-consuming and imprecise. This development marks a pivotal shift towards more accurate and efficient methodologies in submarine cable path planning.

The major contributions of this paper are as follows.

1) We propose an APFMM algorithm, which, for the first time, enables high-precision, ultra-long-distance (over 14,000 km) submarine cable path planning, considering various factors affecting cable reliability and cost. Our APFMM algorithm effectively addresses the computationally prohibitive issues associated with the massive data size in extremely large target areas that traditional SFMM encounters, significantly enhancing computational efficiency while improving the accuracy of the planned submarine cable path.
2) Our APFMM algorithm, leveraging the strengths of DDM and MRA, dynamically decomposes the target area and adjusts the resolution of different sub-domains during the APFMM implementation. In contrast to the general PFMMs, our algorithm ensures a more balanced load distribution among threads to some extent, thereby optimizing the utilization of all threads to the greatest extent possible.

3) We investigate the impact of different sub-domain decomposition methods on the performance of PFMMs. Experimental results indicate that the DDM used in our paper, compared to the traditional regular sub-domain division (for example, regular rectangular partition) approach, significantly reduces the frequency of communication between adjacent sub-domains (i.e., the rollback operation frequency [17]), leading to a considerable improvement in computational efficiency.

The remainder of this paper is structured as follows. In Section II, we survey the related works in the field of submarine cable path planning and the parallelization of FMM. We introduce the models used in submarine cable path planning in Section III. The problem of finding the optimal submarine cable path, defined as the one with the minimal total life-cycle cost between two given fixed points on the Earth, is formulated in Section IV. Section V offers an in-depth discussion on the general SFMM and our innovative APFMM proposed to solve the problem defined in Section IV. We then evaluate the performance of APFMM in comparison to SFMM and two other PFMMs through simulations in Section VI. Finally, we draw conclusions in Section VII.

II. Related work

As mentioned in Section I, the prevailing approach to designing cost-effective and reliable submarine cables in the industry relies on a conventional manual method based on expert knowledge [18]. Planners typically harness a wealth of data about the target area, encompassing maps, aerial photos, charts, and satellite gravity bathymetric data. Leveraging commercial planning software tools, they generate preliminary alternative paths that link the start and end points. One such popular software tool is MakaiPlan [19], which generates the cable path based on the "Great Circle" method that provides the shortest path on a sphere. This simple sphere model does not take into account the Earth's surface, which may include mountains and valleys, and it does not consider any natural or man-made risk factors. According to [18], a subsequent preliminary survey is conducted for the preliminary alternative paths to ascertain their feasibility and sensibility. The final step involves meticulously examining all pertinent details along the cable's path and thoroughly comparing the alternatives. Consequently, the path route is determined. This method heavily leans on the subjective judgments of the planners. Owing to constraints of time and resources, planners may not always be able to consider all available alternatives and the entire array of factors that could impact the cost and resilience of submarine cables. Therefore, it may fall short of yielding a near-optimal path.

Several studies have been performed on models and analyses in the context of cables and cable networks. Neumayer *et al.* [20] provided a network that identifies major disruption sites to alleviate disaster impacts. The work of Tran and Saito [21] entailed a risk analysis of network fractures due to seismic events and the development of network links for optimal durability within cost limitations. Meanwhile, Zhao *et al.* [22] utilized the Dijkstra's algorithm for grid-based route analysis, aiming to reduce the total cost along the route by considering elements like cable length and earthquake resistance. Verikios *et al.* [23] utilized the Dijkstra's algorithm to optimize the placement of energy hubs and the routing of cables. Makrakis *et al.* [24] proposed a GIS-based tool that integrates least cost path analysis with multi-criteria decision-making methods to assess whether a proposed submarine cable route can effectively traverse regions prone to geological disasters, such as earthquakes. In [25], Routray *et al.* investigated the shortest path distances between actual nodes in optical transport networks, assessing their impact on accurate fiber cable length estimations within these networks.Zhao *et al.* [26] proposed an improved ant colony optimization algorithm to optimize the cost and risk of submarine cable path planning. However, the ant colony algorithm has certain inherent issues [27]. These issues include slow convergence speed and sensitivity to parameter settings, such as the release rate of pheromones and the weight of heuristic information.

Wang *et al.* [28] addressed a cable path optimization issue, which was framed as a multi-objective optimization challenge on a 2D manifold in 3D space between two global points. The problem was simplified to an Eikonal equation, solved using FMM [9], rather than the constrained the Dijkstra's algorithm used in [29]. FMM's advantage over the Dijkstra's algorithm was numerically shown in [16, 30], and it was proven in [9] to provide an optimal route on a given triangulated manifold. Further exploration of FMM-based optimization techniques for cable networks can be found in [13–15]. For instance, Wang *et al.* [13] examined a submarine cable system's path planning, considering a trunk-and-branch tree topology on the Earth's surface. Notably, latency constraints for different node pairs in the submarine cable topology network were considered in [14], and [15] incorporated the costs associated with branching units and cable landing stations.

The ongoing advancements in seabed exploration, coupled with the continuous refinement of essential data, have substantially enhanced the conditions for precise, ultra-long-distance submarine cable path planning. However, the sheer number of grid points in a target area for a submarine cable exceeding 10,000 kilometers can easily reach billions, posing a massive data size problem that conventional submarine cable path planning methods struggle to handle. This issue is further complicated by the sequential nature of the SFMM, which is not conducive to straightforward parallelization.

Blaise *et al.* [31] attempted to accelerate the path design process of offshore pipeline or cable path planning by developing a parallel Dijkstra's algorithm. However, we have established that FMM is superior to the Dijkstra's algorithm for cable path planning. Unlike the Dijkstra's algorithm, which restricts the path to edges between consecutive grid points at each step, FMM achieves an optimal path for a given triangulated manifold. This superiority has been both theoretically proven in [9] and demonstrated numerically in [16, 30]. Therefore, based on these findings, we prefer to utilize FMM, as previously discussed. Kotas *et al.* [32] introduced a PFMM technique based on static domain decomposition that can be implemented on large-scale parallel high-performance computing (HPC) systems. Akian *et al.* [33] proposed a multi-level FMM

that employs grid approximations and a "highway hierarchy" technique to approximate solutions for static Hamilton-Jacobi-Bellman equations, allowing FMM to be executed in parallel on each level. Another strategy is to utilize a graphics processing unit (GPU), which offers more cores than CPUs and can handle large data quantities in parallel [34]. Huang [35] proposed an improved fast iterative method to solve Eikonal equations, which a GPU can parallelize. Monsegny *et al.* [36] explored efficient FMM implementation on GPUs, but the sequential nature of FMMs makes direct implementation on GPUs a challenging task.

DDM [37] is a prevalent parallelization method that breaks down a large-scale problem into smaller, independently solvable sub-problems, which can be processed in parallel across different computing units. Specifically, in the case of PFMM implementations, DDM partitions the computational domain, such as a target seabed area, into multiple sub-domains. SFMM is then executed independently within each sub-domain, allowing parallel computation of shortest paths. Once all sub-domains have been processed, a suitable reorganization strategy, such as a multilevel strategy or an optimal reorganization strategy, can be employed to assemble the results from all the sub-domains into a comprehensive global result, transforming a problem that would originally require sequential processing of nodes in a specific order, into a series of sub-problems that can be processed concurrently.

However, managing the interfaces between sub-domains is a significant challenge when using DDM. At these boundaries, it is crucial to ensure accurate information transfer to yield a precise global solution. A common approach is to employ a DDM with overlapping regions between sub-domains [38, 39], which requires the management of junctions between sub-domains and necessitating "ghost nodes" to share information. Currently, extensive research on optimal domain decomposition is lacking. Optimal domain decomposition can make the number of communication and rollback operations between sub-domains very small, and the computing load of each sub-domain is close to balance, achieving far better parallel performance with the minimum parallelization overhead [40]. The study in [41] showed that the efficiency of PFMM greatly depends on how the domain is decomposed, and poor performance results from uneven domain decomposition. Adaptive domain decomposition [17] is an enhanced DDM that can automatically adjust the division of sub-domains according to the features of the problem or the solution (e.g., if a sub-domain is more complex or takes longer time, it can be broken down into smaller sub-domains at runtime), making the computational load more balanced across each sub-domain, thereby improving overall computational efficiency.

MRA [42], which analyzes data at multiple scales and is widely applied in fields like image processing [43], can be combined with the DDM in the parallelization of FMM, where MRA guides the domain decomposition to facilitate load balancing and efficient parallel computation. Initially, the computational domain can be roughly decomposed at the coarsest resolution into multiple sub-domains, and these sub-domains are assigned to different threads. After an initial cable path is computed, the resolution of the area around the path is increased locally and finely decomposed, promoting load balancing and efficiency. By iterating multiple times, each iteration further refines the mesh in critical areas, gradually improving the accuracy of the submarine cable path. In [44, 45], MRA was used to accelerate FMM and improve cable path solutions. However, the absence of parallel techniques resulted in increased computation time. An MRA-like multi-mesh approach allowed finer resolution in key areas, leading to coarse-grained parallelization and PFMMs [46]. Shared-memory PFMM approaches based on overlapping DDM were also introduced in [47, 48]. However, these methods assumed a constant velocity function in the Eikonal equation, which is inappropriate for submarine cable path planning, where different sea areas have varying life-cycle costs. For optimal paths, FMM should propagate faster at points with lower costs, enabling quicker path completion.

In conclusion, to the best of our knowledge, no existing scalable PFMM in industry or literature for high-precision, long-distance submarine cable path planning—which considers various cost and risk factors—affects cables while ensuring thread load balancing and reasonable adaptive target domain decomposition. This paper addresses this by introducing an adaptive DDM in combination with dynamic MRA, utilizing the APFMM algorithm to perform high-precision and ultra-long-distance submarine cable path planning and design.

III. Models

This section describes the Earth's surface and life-cycle cost models for our submarine cable path planning.

A. Earth's surface model

We model the 3D Earth's surface using a two-dimensional manifold $\mathbb{M}$, which is triangulated and piecewise-linear, situated within a three-dimensional space $\mathbb{R}^3$. This serves to represent the target area T. Each point on $\mathbb{M}$ is denoted by a three-dimensional coordinate $X = (x, y, z)$, where $z = \xi(x, y)$ corresponds to the elevation at the geographical location (x, y). For a more comprehensive explanation of the Earth's surface modeling, please refer to [16]. An example of the triangulated piecewise-linear two-dimensional manifold is illustrated in Fig. 2. See more details in [6, 16, 28].

B. Life-cycle cost model

The life-cycle cost of a submarine cable encapsulates the cumulative expenses borne throughout the entire duration of its use. It comprises the initial outlay for construction, the recurring costs for maintenance, and the expenses related to any essential repairs.

The upfront cost of constructing a submarine cable is substantial, often tallying up to hundreds of millions of dollars [2]. While cable length chiefly dictates this cost, we must also consider various natural and human-made risks. These risk considerations include geological phenomena such as volcanic eruptions and earthquakes, as well as physical attributes like water depth, seabed slope, sediment hardness and also human activities like fishing and anchoring, and the requirement to circumnavigate environmentally sensitive or prohibited areas.

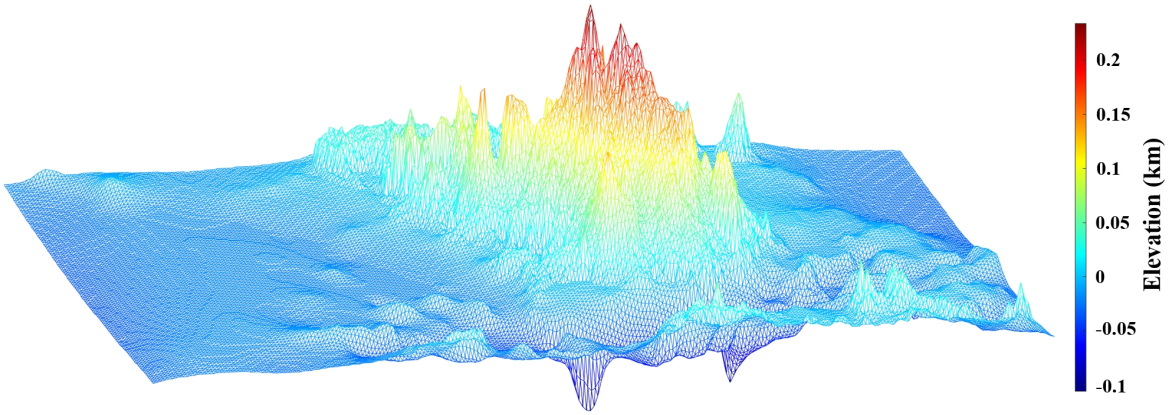

Fig. 2: An example of the Earth's surface modeled by a 2D manifold $\mathbb{M}$ in a 3D space. (Data source: The General Bathymetric Chart of the Oceans, https://www.gebco.net/).

The cable incurs regular maintenance costs upon becoming operational, typically hovering around 3-5% of the initial capital expenditure [49]. The need for repairs, precipitated by natural disasters, human activities, or general wear and tear, can inflate these costs. Repairing a single cable break can demand an investment of hundreds of thousands of dollars.

Specifically, the life-cycle cost per unit length of a submarine cable at a given location X is denoted as $c(X)$. This life-cycle cost is computed as the sum of the weighted cost elements corresponding to various design considerations mentioned above, as stated in (1):

$$c(X) = \sum_{p \in Q} w_p c_p(X), \tag{1}$$

where Q is the set of all design considerations, w_p is the weight assigned to the cost item associated with the p-th design consideration, and $c_p(X)$ represents the cost attributed to the p-th design consideration at location X. The weight values w_p are determined based on the relative significance of each design consideration in the overall cost, with the process of determining these weights explained in Section VI.

The total life-cycle cost, denoted $\mathbb{C}(\gamma)$ for a cable path γ (presumed to be Lipschitz continuous [50]), is calculated by integrating the cost per unit length over the entire length of the cable. The path of the cable, denoted as γ, is described through natural parametrization as a function of arc length s, allowing each point X on the path to be expressed as $X = X(s)$ [51]. Consequently, the cost for a small length ds at location X is $c(X)$ds. This leads to the representation of the total life-cycle cost $\mathbb{C}(\gamma)$ of the cable path γ as shown in (2).

$$\mathbb{C}(\gamma) = \int_0^{l(\gamma)} c(X(s))ds, \tag{2}$$

where $l(\gamma)$ indicates the total length of the cable γ. More details about submarine cable life-cycle models can be found in [6, 16].

IV. Problem Formulation

Given a fixed starting point A and an endpoint B within a target area T, our objective is to design a submarine cable path γ that connects A to B while minimizing the total life-cycle cost, denoted as $\min_{\gamma} \mathbb{C}(\gamma)$. Therefore, we formulate the problem as follows:

$$\begin{aligned} &\min_{\gamma} \mathbb{C}(\gamma) = \min_{\gamma} \int_0^{l(\gamma)} c(X(s))ds, \\ &\text{subject to : } \gamma(A) = A, \gamma(B) = B. \end{aligned} \tag{3}$$

V. The Fast Marching Method

In this section, we describe how we implement APFMM for submarine cable path planning based on our models discussed in Section III to solve the problem formulated in Section IV. FMM converges to the continuous physical (viscosity) solution as the grid step size approaches zero, demonstrating its stability. Additionally, it exhibits a computational complexity of $O(N\log N)$, where N represents the total number of discretized grid points on $\mathbb{M}$ [9].

A. SFMM

As mentioned in [8, 16, 28], we can transform (3) into a nonlinear partial differential equation known as the Eikonal equation. This equation is often used in wave propagation modeling and analyses and can describe a broad range of physical phenomena [9, 52, 53]. Given the complexity of the Eikonal equation, an analytical solution is seldom available.Thus, we lean towards employing a numerical method to extract a numerical solution and utilize FMM to seek the optimal cable path by solving the Eikonal equation.

The general Eikonal equation has the following form.

$$\begin{aligned} ||\nabla u(\mathbf{x})||f(\mathbf{x}) = 1, \quad &\mathbf{x} \in \Omega \setminus \Gamma, \\ \text{subject to : } u(\mathbf{x}) = 0, \quad &\mathbf{x} \in \Gamma \subset \Omega, \end{aligned} \tag{4}$$

where Ω is the target domain in $\mathbb{R}^n$, Γ is the initial interface (or source node), $f(\mathbf{x})$ is the speed function with $f(\mathbf{x}) > 0$, and $||\cdot||$ denotes the Euclidean norm (L2-norm). The physical meaning of the solution $u(\mathbf{x})$ to (4) is the shortest time required to travel from the initial interface (or source node) to point $\mathbf{x}$ within the computational domain Ω at speed defined by the function $f(\mathbf{x})$. In the special case where $f(\mathbf{x}) = 1$,

the solution to (4) represents the distance map within the computational domain Ω.

For the submarine cable path planning scenario with a starting point A and endpoint B in a target area T, the Eikonal equation can be written as:

$$\begin{aligned} &||\nabla\phi\,(X)\,|| = c(X), \quad X \in \mathbb{M} \setminus A, \\ &\text{subject to}: \phi\,(A) = 0, \end{aligned} \tag{5}$$

where X is the grid point on the triangulated manifold $\mathbb{M}$ of target area T, $\phi(X)$ represents the minimal total life-cycle cost for a cable path from the starting point A to point X. The life-cycle cost at point X, denoted as $c(X)$, is defined in Equation (1).

To solve (5), we start with a simple case. Taking a two-dimensional orthogonal grid (with a grid spacing h) as an example (see Fig. 3(a)), and replacing the gradient term on the left side of (5) with a first-order approximation yields [52]:

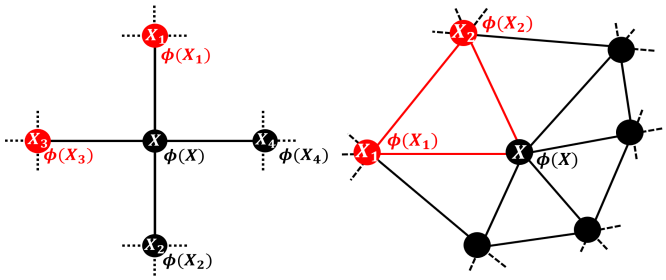

(a) An example of a two-dimensional orthogonal grid with a grid spacing h.

(b) An example of a triangulated grid. Note that these triangles are not necessarily in the same plane.

Fig. 3: Two different grids.

$$\begin{aligned} &\max\left(\phi(X)-\phi(X_1),\phi(X)-\phi(X_2),0\right)^2 \\ &+\max\left(\phi(X)-\phi(X_3),\phi(X)-\phi(X_4),0\right)^2 = \frac{h^2}{c(X)^2}. \end{aligned} \tag{6}$$

We assume $\phi(X_1) = \min\left(\phi(X_1),\phi(X_2)\right)$, $\phi(X_3) = \min\left(\phi(X_3),\phi(X_4)\right)$, then we have:

$$\left(\phi(X)-\phi(X_1)\right)^2 + \left(\phi(X)-\phi(X_3)\right)^2 = h^2/c(X)^2. \tag{7}$$

By further solving (7) [52], we derive the solution:

$$\phi(X) = \begin{cases} \dfrac{\phi(X_1)+\phi(X_3)+\sqrt{\frac{h^2}{c(X)^2}-\left(\phi(X_1)-\phi(X_3)\right)^2}}{2}, \\ \qquad\qquad \text{for } |\phi(X_1)-\phi(X_3)| \le \frac{h}{c(X)}, \\ \min\left(\phi(X_1),\phi(X_3)\right)+\frac{h^2}{c(X)^2}, \\ \qquad\qquad \text{for } |\phi(X_1)-\phi(X_3)| > \frac{h}{c(X)}. \end{cases} \tag{8}$$

Now, considering the triangulated manifold of our Earth's surface model mentioned in Section III-A, we implement FMM on the triangulated manifold (see Fig. 3(b)) to solve the Eikonal equation.

For the triangle comprises of the grid points X_1, X_2, and X in Fig. 3(b), one has [54]:

$$\left\langle \nabla\phi(X), \overrightarrow{XX_i} \right\rangle \approx \phi(X)-\phi(X_i), i \in \{1,2\}, \tag{9}$$

where $\langle\cdot\rangle$ denotes the inner product of vectors, and $\overrightarrow{XX_i}$ represents the vector from point X to point X_i.

In this context, the Eikonal equation can be approximated as the following quadratic equation:

$$(\alpha^{\mathrm{T}}\mathcal{P}\alpha)\phi(X)^2 + (2\alpha^{\mathrm{T}}\mathcal{P}\beta)\phi(X) + \beta^{\mathrm{T}}\mathcal{P}\beta = 1/c(X)^2, \tag{10}$$

where $\alpha = [1;1]$, $\beta = -[\phi(X_1);\phi(X_2)]$, $\mathcal{P} = (\mathcal{Q}\mathcal{Q}^{\mathrm{T}})^{-1}$, $\mathcal{Q} = [X-X_1; X-X_2]$. To be more precise, $\mathcal{Q}$ represents the two side vectors of a triangle that lies on a plane. In particular, the first column of vectors represents the vector from grid point X to X_1, while the second column represents the vector from grid point X to X_2. These vectors originate from grid point X and form a matrix $\mathcal{Q}$, which can be considered a matrix in a coordinate system with X as the origin. $\mathcal{P}$ is a commonly used geometric quantity that denotes the length ratio of the inner bisector of the angle formed by three grid points on the plane. Specifically, $\mathcal{P}$ represents the ratio of the lengths of the bisectors of the interior angles of a triangle.

By solving (10), one derives the solution of (5). By iteratively updating the ϕ-values of grid points with unknown values, using the ϕ-values of neighboring grid points with known values, the FMM is able to propagate forward and compute solutions efficiently. See [9, 52–54] for more details.

The implementation process of SFMM for submarine cable path planning is described in the following two-stage procedure.

1) Launch a wave from the initial point A, which spreads outwards until it reaches the final point B. As it expands, each point is assigned a value equal to the accumulated life-cycle cost from A to that point. This is done by setting the speed of expansion from each grid point as the inverse of its life-cycle cost.
2) Commence a reverse journey from B back to A, utilizing the life-cycle cost data collected in the first step. This does not necessarily mean revisiting the grid points in a reverse sequence. The FMM enables the reverse path to traverse the edges of the triangulated manifold in a direction that corresponds to the steepest descent in $\phi(X)$.

Algorithm 1 provides the pseudocode of SFMM.

B. APFMM

The parallelization approaches of FMM based on DDM in various existing publications [46–48] are similar to each other in that they all involve the two key steps: (1) domain decomposition and (2) parallelization in each sub-domain.

1) The first step: domain decomposition: In this step, the initial computation domain is broken down into several sub-domains. In this context, the target area T, which is the initial computational domain in (5), is divided into n sub-domains $T_1, \cdots, T_n$ and assigned to n threads with each sub-domain T_i corresponding to one thread labeled π_i, $i \in \{1,2,\cdots,n\}$. In this context, the initial manifold $\mathbb{M}$ is also divided into n sub-manifolds in the meanwhile, with each sub-manifold $\mathbb{M}_i$ corresponding to the sub-domain T_i.

Each sub-domain T_i is externally surrounded by a ghost layer g_i and features a border layer b_i that is situated within its domain that shares a border with its ghost layer g_i. The border

Algorithm 1: The SFMM for point-to-point submarine cable path planning.

Input: Starting point A and endpoint B, w_p and $c_p(X)$ for $p \in Q, X \in \mathbb{M}$.
Output: The optimal cable path γ which connects A and B with minimal total life-cycle cost.

Initialization: $\phi(X) = \infty$ for all $X \in \mathbb{M} \setminus A$, $\phi(A) = 0$;
  $\mathcal{S} = \{X | X \in \mathbb{M} \setminus A\}$ // the set of *far* grid points that are unprocessed;
  $\mathcal{C} = \{A\}$ // the set of *accepted* grid points, where only the starting point A is involved;
  $\mathcal{N} = \emptyset$ // the set of *considered* grid points that are neighboring to the grid points in $\mathcal{C}$;
Find the nearest neighbors (one grid point away) of A and move them to $\mathcal{N}$;
while $\mathcal{N} \neq \emptyset$ **do**
  Calculate ϕ values for every grid point in $\mathcal{N}$ using the grid points in $\mathcal{C}$ and (10);
  Find $X^{\min} \in \mathcal{N}$ with smallest $\phi(X^{\min})$, if there are more than one grid points with $\phi(X^{\min})$, pick one arbitrarily;
  Move $X^{\min}$ from $\mathcal{N}$ to $\mathcal{C}$;
  for *every nearest neighbor (one grid point away) grid point* X' *of* X^{min} *in* $\mathcal{S}$ **do**
    Move X' from $\mathcal{S}$ to $\mathcal{N}$;
  end
  for *every neighbor grid point* X'' *of* X^{min} *in* $\mathcal{N}$ **do**
    for *every triangle* t *on the manifold of* T *whose vertexes contains* X'' **do**
      Calculate $\phi_t(X'')$ on the triangular patch, using the grid points in $\mathcal{C}$ and (10);
    end
    Find the minimal $\phi_t(X'')$ and write down as $\phi^{\text{new}}(X'')$;
    $\phi(X'') = \min(\phi(X''), \phi^{\text{new}}(X''))$;
  end
end

layer b_i of T_i is overlapped with its neighboring sub-domain's ghost layer. Fig. 4 illustrates the overlapping DDM of two sub-domains. Fig. 4(a) demonstrates the decomposition of initial domain T into two sub-domains, T_1 and T_2. The border layer b_1 within T_1 overlaps with the ghost layer g_2 that surrounds T_2, and likewise, the border layer b_2 within T_2 overlaps with the ghost layer g_1 that surrounds T_1, see in Fig. 4(b). Fig. 4(c) represents the data exchange process between T_1 and T_2. Specifically, the grid points located within the overlapping regions b_1/g_2 and b_2/g_1 (as depicted in Fig. 4(b)) may have their ϕ-values updated either by the FMM process in T_1 or the FMM process in T_2. This update will only occur if the updated value is smaller than the existing value, thereby adhering to the FMM's upwind principle.

Data exchange between neighboring sub-domains is crucial because it ensures that grid points on the boundaries of each sub-domain can access necessary information from neighboring sub-domains, which is essential for accurate wavefront propagation of FMM. This exchange of boundary data is vital not only for maintaining the accuracy and consistency of computations across the entire computational domain but also enhances overall efficiency. By allowing multiple threads to work concurrently and exchange relevant data as needed, the system can effectively synchronize computations and minimize errors, leading to more reliable and quicker results.

2) The second step: parallelization in each sub-domain: Once the domain has been decomposed, the second step is to parallelize by performing SFMM independently on each sub-domain. To illustrate the parallelization process in detail, we will use the overlapping DDM depicted in Fig. 4 as an example and describe the implementation of PFMM in T_1 in Table I.

TABLE I: The implementation of PFMM in sub-domain T_1.

Step	Actions
(A)	Initialize by calculating the ϕ-value at each grid point on the interface (or source node), labeling them as *accepted*. Adjacent grid points to these *accepted* ones are regarded as *considered* while the remaining ones (including the grid points in the ghost layer g_1) are classified as *far*. Assign an infinite ϕ-value to all *considered* and *far* grid points.
(B)	Determine the ϕ-value for each *considered* grid point by solving (10).
(C)	Inspect if the ϕ-value of an *accepted* grid point within the ghost layer has been replaced by a smaller value, say ϕ'. If true, rollback by designating all grid points in $T_1 \cup g_1$ with ϕ-value not less than ϕ' as *considered*.
(D)	Identify the grid point X' with the minimal ϕ-value in $T_1 \cup g_1$ and mark it as *accepted*.
(E)	Tag all the *far* grid points in $T_1 \cup g_1$ that are adjacent to X' as *considered*.
(F)	Recompute the ϕ-value for all the *considered* grid points in $T_1 \cup g_1$ by solving (10).
(G)	Verify if X' is within b_i and, if so, interact with adjacent sub-domains whose ghost layers overlap with b_i, updating the status of X' in the relevant sub-domains.
(H)	Repeat Steps (C)-(F) until all the grid points in T_1 have been denoted as *accepted*.
(I)	Pause until the other sub-domains $T_i, i \in \{2, 3, 4\}$ have marked all their local grid points $X, X \in T_i$ as *accepted*. Meanwhile, if a grid point in g_1 is updated with a different ϕ-value by other sub-domains, revert to Step (C).

The parallelism in Steps (A) and (C)-(F) in Table I with those in the SFMM is apparent, serving as the initialization and propagation stages, respectively. However, a distinguishing feature in PFMM is including a rollback operation in Step (C) for grid points with ϕ-values exceeding the newly computed ϕ'. This precaution is necessary since ϕ-values surpassing ϕ' may be inaccurate due to their potential reliance on ϕ', consid-

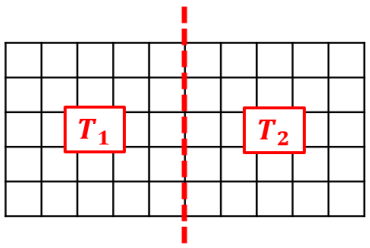

(a) The initial domain T is divided into two sub-domains T_1 and T_2 by the red dash line.

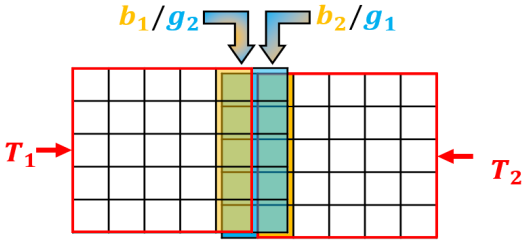

(b) Overlapping between sub-domain T_1 and T_2.

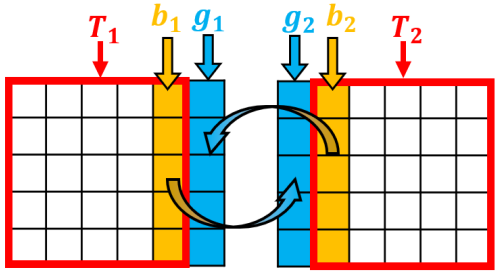

(c) Data exchange between sub-domains.

Fig. 4: The schematic depicting the overlapping DDM.

ering that FMM propagates from the smaller values to larger values [9]. Thus, to ensure algorithmic consistency, we need to revert the status of the corresponding grid points with ϕ-values exceeding ϕ' for a fresh computation of their ϕ-values. Notably, during each rollback operation, we merely alter the labels of the grid points (those with ϕ-values surpassing ϕ') from *accepted* to *considered*, without tampering with their ϕ-values. The rationale behind this approach is that any future update will either minimize its value or leave it intact, as stated by Herrmann [40]. By abiding by this principle, we can save significant computation time as it obviates the need to recompute the ϕ-values of these points.

However, these rollback instances might occur repeatedly even for the same grid points, thereby imposing additional communication demands and increasing computational expenses due to the necessity of visiting all the grid points within the sub-domain T_1 and the ghost layer g_1 for every rollback. Therefore, the rollback operation significantly impacts parallel efficiency, and the frequency of their occurrence is related to the method used for sub-domain partitioning [17, 55].

As a simple two-dimensional illustrative example of (4),

$$T = [0,5]^2, c(X) \equiv 1, A = (0,0), \phi(A) = 0, \qquad (11)$$

where we consider the problem of cable path planning in a domain $T = [0,5]^2$ with the starting point as $A = (0,0)$ and assume that the propagation speed is constant throughout the domain, with $c(X) \equiv 1$. This simplifying assumption ignores the fact that different grid points may have different life-cycle costs. However, it allows us to analyze the optimal region decomposition method straightforwardly.

Fig. 5 illustrates the solution $\phi(X)$ to (11) and its corresponding level sets, where FMM commences from the starting point A, propagating fastest along the characteristic curves perpendicular to the level sets of $\phi(X)$, until it reaches the endpoint $B = (5,5)$. On this basis, an optimal decomposition occurs when all boundaries of the sub-domains align with these characteristic curves, as shown in Fig. 6(a). In such a scenario, the propagation does not cross the boundaries frequently, eliminating additional data communication burden in a way. This burden may arise from repeated access (both reading and writing) to grid points in overlapping regions and potential rollback operations. However, if all the boundaries of sub-domains are orthogonal to the characteristics [56], as depicted in Fig. 6(b), computation tends to become serial, irrespective of the domain decomposition.

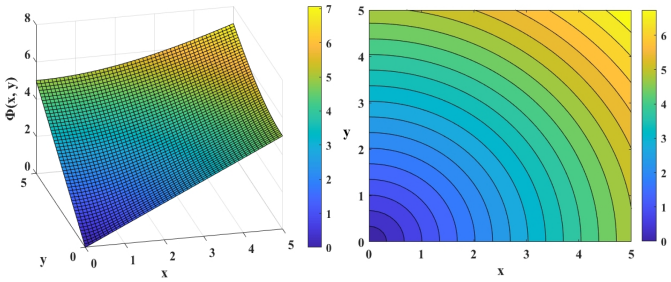

(a) Solution $\phi(X)$. (b) Level sets.

Fig. 5: Solution of (11) and its level sets.

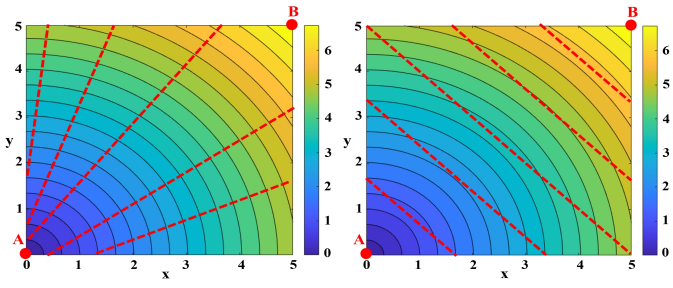

(a) A "good" domain decomposition. (b) A "bad" domain decomposition.

Fig. 6: Different domain decompositions for (11): $c(X) \equiv 1$.

It is worth noting that in practice, the life-cycle cost $c(X)$ for each grid point within the domain varies due to different laying conditions at different locations, resulting in varying life-cycle costs. Therefore, the level set of the target area is often very tortuous and irregular, see Fig. 7, which is different from the level sets shown in Fig. 6, making it challenging to divide sub-domains exactly along the characteristic curves.

However, since our objective is to connect the given starting point A and endpoint B on $\mathbb{M} \in \mathbb{R}^3$, it is predictable that dividing sub-domains along the direction connecting A and B is better than dividing them perpendicular to the direction

connecting the origin and destination. This is because dividing the sub-domains along the fastest propagation direction of the FMM can reduce the communication frequency and the frequency of rollbacks, resulting in higher parallelization efficiency.

In Fig. 7, we observe the vector that stretches from the starting point A to the endpoint B, as depicted by the black arrowed line. We then decompose the domain in different ways: parallel and perpendicular to this direction, as shown in Fig. 7(a) and Fig. 7(b) respectively. It is apparent that the number of sub-domains that need to be crossed for FMM to propagate from A to B in Fig. 7(b) exceeds that in Fig. 7(a).

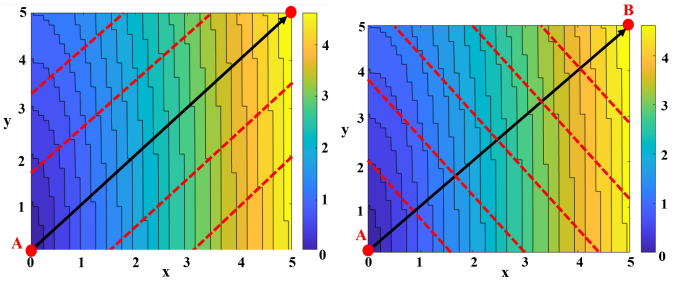

(a) A "good" domain decomposition. (b) A "bad" domain decomposition.

Fig. 7: Different domain decompositions for (11) with various $c(X)$ values.

On this basis, we propose an adaptive parallel FMM algorithm based on adaptive domain decomposition and MRA. Table II and Algorithm 2 provide the details of this algorithm and its pseudocode, respectively.

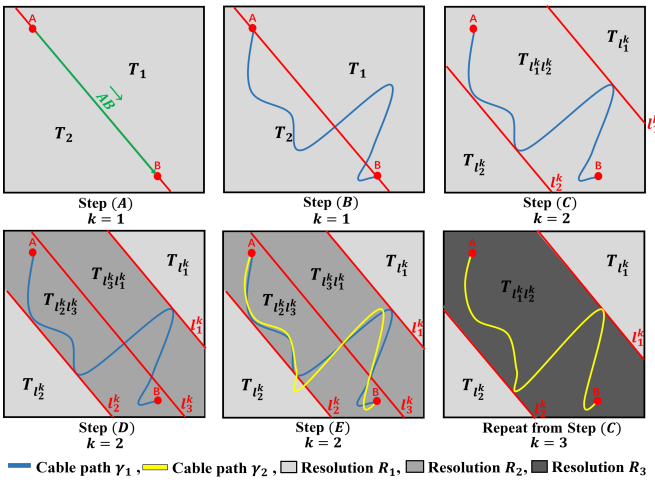

Fig. 8: Implementation of APFMM in submarine cable path planning. Darker regions indicate areas of higher resolution.

In Step (C) of Table II, we initially identify two decomposition lines, l_1^k and l_2^k, which are parallel to $\overrightarrow{AB}$ and possess the minimum distance $\mathcal{D}_{\gamma_{k-1}}(l_1^k, l_2^k)$ between l_1^k and l_2^k that can enclose the path γ_{k-1}. As the optimal path γ_{k-1} derived in the prior iteration is entirely contained within the region $T_{l_1^k l_2^k}$, this suggests that the region $T_{l_1^k l_2^k}$ holds heightened importance for us. Consequently, we increase the resolution in the area

TABLE II: Implementation of APFMM for point-to-point submarine cable path planning.

Step	Actions
(A)	Initialize the decomposition index $k = 1$. Assign an extremely low initial resolution (denoted as R_1) to the initial region T. Divide the initial region T into two sub-domains T_1 and T_2, along the direction defined by the starting point A and the endpoint B (denoted as $\overrightarrow{AB}$).
(B)	Allocate the two sub-domains T_1 and T_2 to two threads, respectively. Execute FMM in parallel from the starting point A for each sub-domain, as described in Table I. Denote the resulting optimal cable path as γ_1.
(C)	Increase the decomposition index $k = k + 1$. Define $L = \{l \mid l \parallel \overrightarrow{AB}\}$ as the set of all domain decomposition lines parallel to $\overrightarrow{AB}$. Let $\mathcal{D}_{\gamma_k}(l_x, l_y)$ denote the distance between two domain decomposition lines l_x and l_y in L that enclose the cable path γ_k. The area between two decomposition lines l_x and l_y is denoted as $T_{l_x l_y}$. Identify l_1^k and l_2^k by solving $(l_1^k, l_2^k) = \underset{l_x, l_y \in L}{\operatorname{argmin}} \mathcal{D}_{\gamma_{k-1}}(l_x, l_y)$. For the initial area T excluding $T_{l_1^k l_2^k}$, use $T_{l_1^k}$ and $T_{l_2^k}$ to denote the two sub-domains bordering the decomposition lines l_1^k and l_2^k, respectively.
(D)	Increase the resolution of the area $T_{l_1^k l_2^k}$ (denoted the increased resolution as R_k), and further divide it equally into 2^{k-1} sub-domains $(T_{l_1^k l_3^k}, T_{l_3^k l_4^k}, ..., T_{l^k_{3+2^{k-1}-1} l_2^k})$, aligned with the direction of $\overrightarrow{AB}$. The decomposition lines are labeled as $l_3^k, l_4^k, ..., l^k_{3+2^{k-1}-1}$.
(E)	Assign these 2^{k-1} sub-domains along with the sub-domains $T_{l_1^k}$ and $T_{l_2^k}$ obtained in Step (C) (making a total of $2^{k-1}+2$ sub-domains) one-to-one to $2^{k-1}+2$ threads. Execute FMM in parallel as described in Table I. Specifically, for each sub-domain, the grid point X^* where the path γ_{k-1} first enters this sub-domain is set as the sour of FMM and its corresponding ϕ-value, $\phi(X^*)$, is used for the FMM propagation. The resulting optimal cable path is denoted as γ_k.
(F)	Reiterate Steps (C)-(E) until the region $T_{l_1^k l_2^k}$ achieves the highest possible data resolution, or the total number of sub-domains for the next decomposition $2^k + 2$ surpasses the predetermined maximum number of available threads.

$T_{l_1^k l_2^k}$, and partition the area $T_{l_1^k l_2^k}$ into 2^{k-1} equally-sized sub-domains along the direction of $\overrightarrow{AB}$. This ensures that each sub-domain stemming from the area $T_{l_1^k l_2^k}$ can maintain an equivalent number of grid points as the resolution increases, thereby facilitating a balanced load distribution among the threads managing these sub-domains as much as possible. For the initial area T outside $T_{l_1^k l_2^k}$, we refrain from increasing the resolution given that the path from the previous iteration did not traverse these areas, thereby avoiding unnecessary computational load.

Following the division of all sub-domains, we proceed to Step (E) of Table II, where we execute FMM in parallel in each sub-domain, as described in Table I. As the area $T_{l_1^k l_2^k}$ between the two decomposition lines l_1^k and l_2^k encompasses the path γ_{k-1}, and the distance d between l_1^k and l_2^k is minimal, we can guarantee that at least one grid point on the path γ_{k-1} is present in each sub-domain. Given this, and considering the upwind propagation characteristics of FMM [9], we designate the grid point in a sub-domain where the path γ_{k-1} first enters in this sub-domain as the source point of FMM propagation in this sub-domain. It is worth noting that for areas outside the

Algorithm 2: Implementation of APFMM for Point-to-Point Submarine Cable Path Planning.

Input: Starting point A and endpoint B, w_p and $c_p(X)$ for $p \in Q, X \in \mathbb{M}$, the maximum number of available threads n, an extremely low initial resolution R_1, and the highest available data resolution R_h.

Output: The optimal cable path γ_k which connects A and B with minimal total life-cycle cost.

Initialization: $k = 1$ and assign an extremely low initial resolution R_1 to the initial region T.
Divide the T into two sub-domains T_1 and T_2 along $\overrightarrow{AB}$;
Allocate T_1 and T_2 to π_1 and π_2 respectively;
Execute the PFMM as shown in Table I for T_1 and T_2 from A and to get the optimal cable path γ_1;
while *the region* $T_{l_1^k l_2^k}$ *has not achieved the highest possible data resolution and* $2^k + 2 < n$ **do**
    $k = k + 1$;
    $(l_1^k, l_2^k) = \underset{l_x, l_y \in L}{\operatorname{argmin}} \mathcal{D}_{\gamma_{k-1}}(l_x, l_y)$;
    Increase the resolution of the area $T_{l_1^k l_2^k}$ (denoted as R_k);
    Divide $T_{l_1^k l_2^k}$ equally into 2^{k-1} sub-domains ($T_{l_1^k l_3^k}, T_{l_3^k l_4^k}, ..., T_{l^k_{3+2^{k-1}-1} l_2^k}$);
    Assign all 2^k sub-domains $T_{l_1^k l_3^k}, T_{l_3^k l_4^k}, ..., T_{l^k_{3+2^{k-1}-1} l_2^k}$, $T_{l_1^k}$ and $T_{l_2^k}$ one-to-one to $2^{k-1} + 2$ threads $\pi_1, \pi_2, \pi_3, ..., \pi_{2^k}$;
    Execute FMM in parallel for all sub-domains as described in Table I to get the optimal cable path γ_k. Specifically, for each sub-domain, the FMM propagates from X^* with $\phi(X^*)$.
end

decomposition l_1^k and l_2^k, namely $T_{l_1^k}$ and $T_{l_2^k}$, we continue to use the lowest initial resolution R_1 rather than reducing the resolution to zero (i.e., removing points within these areas). This is because we cannot guarantee that the path obtained in the next iteration will not enter these areas.

It should be noted that since APFMM dynamically decomposes sub-domains and selectively enhances resolution in specific areas during each iteration to improve accuracy and path quality, the stability and convergence of APFMM are closely linked to this iterative process. As outlined in Table II (F), we have implemented mechanisms to prevent the algorithm from running indefinitely. Specifically, the iterative process in APFMM is designed to halt under two circumstances: either when the highest possible data resolution is achieved or when the number of sub-domains for the next decomposition exceeds the predetermined maximum number of available threads. These conditions ensure that the APFMM does not continuously increase the complexity of the problem but instead concentrates on achieving the best possible solutions within the confines of the available hardware resources and datasets. The defined termination points are pivotal, as they ensure that the algorithm remains computationally manageable and converges to a dependable solution within a feasible timeframe, leveraging the quality and capacity of the available computational resources.

Fig. 8 illustrates the execution process of APFMM as detailed in Table II. Each sub-figure is annotated below with the execution steps corresponding to it, as well as the current decomposition index k. Concurrently, the darker the area, the higher its resolution. The blue curve represents the optimal path computed in the initial iteration, while the yellow curve signifies the optimal path determined following the second sub-domain re-decomposition. During the APFMM process, MRA and DDM are dynamically integrated. MRA guides the domain decomposition to achieve load balancing and efficient parallel computation. Initially, the computational domain is at the coarsest resolution R_1. After computing the initial cable path, the resolution around the path's surrounding area (namely the areas between l_1^k and l_2^k) is increased locally for finer decomposition, thus enhancing load balancing and efficiency. Through multiple iterations (continuously repeating Steps (C)-(E) from Table II), the grid in critical areas is refined progressively, thereby progressively enhancing the precision and quality of the submarine cable path solution.

VI. Application

A. General information

In this section, we demonstrate the application of our APFMM by addressing a practical scenario of point-to-point submarine cable path planning. The starting point of our path is positioned at South Gorge Headland, Australia, located at coordinates ($27°26'13''$S, $153°32'44''$E) and represented by a red circle. Conversely, the endpoint is at the Arch of Cabo San Lucas, Mexico, at coordinates ($22°52'31''$N, $109°53'42''$W), denoted by a black circle. The geographical context of the starting point and endpoint is illustrated in Fig. 9.

B. Design considerations

In our application, we incorporate various design considerations, each assigned a specific weight value, as detailed in Table III. These weights are adopted from [6], where they were derived from an existing real-world manually-designed cable by experts called "Southern Cross NEXT" located in the Pacific Ocean and were shown to balance all considerations with realistic priorities effectively [6].

- The basic construction cost is associated with the length of the cable and includes the cost of repeaters installed at nearly regular intervals to counteract signal attenuation [8]. Consequently, for simplicity in our analysis,

we presume that the basic construction cost is directly proportional to the length of the submarine cables.

- Geological hazards considered in this study include earthquakes and volcanic eruptions. Earthquakes can lead to considerable shifts in the seabed and can destabilize the sediment through processes like liquefaction, surface faulting, and landslides [57]. Such events pose a serious risk to submarine cables. Similarly, volcanic eruptions threaten these cables by means of lava flows and the descent of hot debris [58]. We source earthquake data from the United States Geological Survey (USGS, https://earthquake.usgs.gov/), and information on volcanic eruptions from the National Oceanic and Atmospheric Administration (NOAA, https://www.ngdc.noaa.gov/). It is important to note that only earthquakes with magnitudes greater than 4.5 over the past 50 years are considered in our analysis.
- Seabed slopes bring gravitational forces that can lead to hazards like debris flows [59]. In steep areas, it is often essential for cable routes to cross the slope orthogonally and limit directional changes. This approach minimizes the lateral contact area between the cable and the seabed, reducing potential risks [16].
- Deeper waters typically face fewer threats from human activities [57]. For instance, cables in shallow waters are usually double-armored and buried up to 1.5 meters deep to ensure adequate protection, which incurs additional costs [16].
- Fishing and anchoring represent the main anthropological hazards leading to cable faults. Statistical data indicates that globally, there are over 100 cable faults each year, with about two-thirds of these faults caused by fishing and anchoring activities [2]. As previously noted, the risk to cables from these activities diminishes with increasing water depth.
- In our study, we consider protected areas, particularly seagrass and coral habitats, because cable deployment and repair operations could negatively impact vulnerable species inhabiting these seabed ecosystems [16, 59]. It is crucial that laying submarine cables does not harm the marine ecological environment. Consequently, cable routes should be designed to minimize disturbance and avoid environmentally sensitive areas as much as possible.

The global gridded terrain data for both oceanic and terrestrial environments are obtained from the General Bathymetric Chart of the Oceans (GEBCO, https://www.gebco.net) at intervals of 15 arc-seconds. This dataset facilitates the construction of a triangulated manifold model $\mathbb{M}$, with the nearest distance between adjacent grid points reaching about 60 meters. Additionally, the GEBCO data are utilized to assess seabed slope and water depth. Given that the costs associated with anthropogenic hazards, namely fishing and anchoring activities in this study, correlate with water depth [16], the GEBCO data also helps with the calculation of the costs of such hazards. The data for protected areas are sourced from the World Conservation Monitoring Centre (WCMC, https://data.unep-wcmc.org/datasets/).

For a detailed discussion of the cost calculations of the aforementioned considerations and the choice of weights assigned in Table III, please refer to [6], where these weights have been demonstrated to be effective in reflecting real-world priorities based on publicly available data. Note that practitioners have the flexibility to adjust these weights or add new design considerations based on specific conditions. Practical path planning involves additional considerations beyond what we considered in this paper in our life-cycle cost model, such as sediment hardness, turbulent currents, undersea oil exploration, and the presence of existing infrastructures. Moreover, the use of detailed or high-resolution private datasets can significantly impact the outcomes of cable path planning. While different weight values and additional considerations can influence the final path planning results, it is crucial to note that the solutions presented here are optimal, given the available data and weight values [9, 17, 32, 52–54]. Incorporating comprehensive data from private sources is expected to enhance solution quality, as optimizations would be recalibrated based on this richer dataset. Our goal is not to replace the current manual methods of cable path planning but to augment the precision and effectiveness of the outcomes using our APFMM, thereby generating automated, high-precision cable path planning solutions.

It should be noted that our path planning is performed on a manifold $\mathbb{M}$, consisting of grid points spaced according to the chosen resolution. Grid points within obstacles, such as marine protected areas, are assigned an infinite cost, ensuring that paths do not traverse these zones. Instead, paths will be routed around the periphery of these obstacles. Given the grid spacing, which is tens of meters apart based on our highest resolution, paths are generally kept at a sufficient safe distance from obstacles. When using higher-resolution data, even though the grid points are closer, we can manage to maintain safety by setting buffer zones around obstacles before path planning. This ensures the paths are still safely distanced from actual obstacle locations. In essence, our path-planning approach optimizes routes based on available data, serving as a reference or benchmark. Practitioners may further adapt these routes in real-world applications, enhancing safety measures as necessary in critical areas.

TABLE III: Design considerations and the corresponding weight values.

Design considerations	Weight value
Basic construction cost	0.1695
Geological hazards	0.3852
Seabed slope	0.1645
Water depth	0.0215
Anthropological hazards	0.0739
Protected areas	0.1851

C. Numerical results

In this section, we first use APFMM to calculate the optimal cable path connecting the starting point A and the endpoint B until the highest available resolution data is reached. Fig. 10

TABLE IV: Simulation results for APFMM.

Decomposition index k	Total length of cable path γ_k (km)	Total life-cycle cost of cable path γ_k ($\times 10^6$ \$)	Average distance between two adjacent grid points (km)	Number of sub-domains (threads)	*RF* ($\times 10^{-4}$)
1	14200.00	397.6001	53.7174	2	0
2	14545.49	407.2737	22.5447	4	0.0097
3	14566.50	407.8620	9.5867	6	0.0110
4	14518.82	406.5269	2.1034	10	0.0272
5	14533.46	406.9368	0.4277	18	0.0494
6	14515.52	406.4344	0.1545	34	0.0765
7	14516.94	406.4927	0.0671	66	0.1201

shows part of the APFMM solution process, and Table IV shows the detailed results for each implementation cycle of APFMM. All the results were obtained using a 12th Gen Intel(R) Core(TM) i9-12900HX (64GB RAM) for running the codes in Matlab R2023b using the Parallel Computing Toolbox.

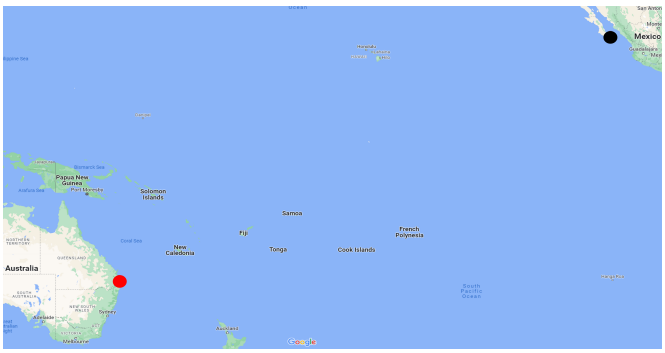

Fig. 9: The target region in Google Earth.

In our application, APFMM utilizes a maximum of 66 sub-domains and parallel threads. This choice is justified by two key factors. On the one hand, at the 7th iteration (decomposition index $k = 7$), the GEBCO's global gridded terrain dataset we used reaches its highest available resolution accuracy, meaning we have achieved the goal of finding the optimal path using APFMM with the given available data. On the other hand, we observed a decline in computational efficiency with the iteration index increased, as indicated by the increasing *RF* index in Table IV. This demonstrates that merely increasing the number of parallel threads and sub-domain divisions does not consistently yield performance benefits. Therefore, our APFMM concludes at the 7th iteration, utilizing 66 sub-domains and threads.

In Fig. 10(a), we first establish a manifold for the initial region, T, along the direction connecting the starting point A and the endpoint B, utilizing the lowest resolution R_1. We subsequently divide T into two sub-regions, T_1 and T_2. By executing FMM in parallel in both T_1 and T_2, using A as the source, we obtain the path γ_1, depicted in Fig. 10(b).

In Fig. 10(b), we identify the partition lines l_1^k and l_2^k, which can encompass the path γ_1 and are parallel to $\overrightarrow{AB}$, with a minimum distance d^k between each other. As we progress to Fig. 10(c), we increment the domain decomposition index k by one and initiate the subsequent decomposition. We increase the resolution of the region $T_{l_1^k l_2^k}$ in Fig. 10(b) by a factor of two (denoted as R_2), dividing it equally into two sub-domains marked as $T_{l_1^k l_3^k}$ and $T_{l_2^k l_3^k}$.

By executing FMM in parallel across all four sub-regions in Fig. 10(c), we derive the path γ_2, as illustrated in Fig. 10(d). The operations conducted in Fig. 10(e) and Fig. 10(f) mirror those in Fig. 10(b) and Fig. 10(c). However, compared to Fig. 10(b), the resolution of the region $T_{l_1^k l_2^k}$, situated between the partition lines l_1^k and l_2^k in Fig. 10(f), is further amplified (denoted as R_3) and subdivided into four equidistant sub-domains. Fig. 10(g) presents the optimal path γ_3 obtained under the sub-domain decomposition scenario and resolution settings depicted in Fig. 10(f).

Ultimately, by perpetually executing the sequence of "re-decomposition - resolution enhancement - path solving" (i.e., from Fig. 10(b) to Fig. 10(d)), we arrive at the final submarine cable path depicted in Fig. 10(h).

It should be noted that even though the resolution of the region $T_{l_1^k l_2^k}$ between l_1^k and l_2^k consistently increases (thus leading to an expansion in the number of grid points in this region), the number of sub-domains divided between the decomposition lines l_1^k and l_2^k concurrently escalates. This strategy ensures a minimal load disparity between the thread responsible for the sub-domains within l_1^k and l_2^k, and the threads responsible for the sub-domains outside l_1^k and l_2^k (which consistently utilize the initial low resolution R_1). Maintaining a balanced load across all threads aids in enhancing parallel efficiency and accelerating the implementation of APFMM.

To analyze the advantage of our APFMM, we compare APFMM with the traditional SFMM as well as two PFMMs named PFMM-I and PFMM-II. These two PFMMs employ static domain decomposition strategies for parallelization, which are frequently mentioned in existing literature [32, 40, 41, 46, 47, 55]. Specifically, for PFMM-I, we employ orthometric (horizontal and vertical) decomposition lines, as considered in [32, 40, 41, 46, 47], to divide the initial domain T into 66 rectangular sub-domains. These sub-domains are then assigned to 66 threads, matching the thread count used by APFMM in its final iteration before termination. In PFMM-II, as mentioned in [46, 55, 56], the different angles between the decomposition lines and the direction of FMM propagation affect the frequency of rollbacks during the FMM parallelization process, and ultimately influence the parallel efficiency of FMM. Thus, we use domain decomposition lines that are perpendicular to the vector $\overrightarrow{AB}$ to divide the domain T into 66 sub-domains, which are also assigned to 66 threads. This division differs from the method used in

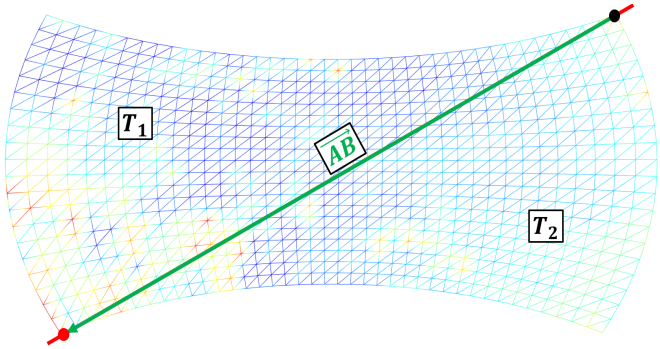

(a) $k = 1$. Dividing the initial region T into two along $\overrightarrow{AB}$.

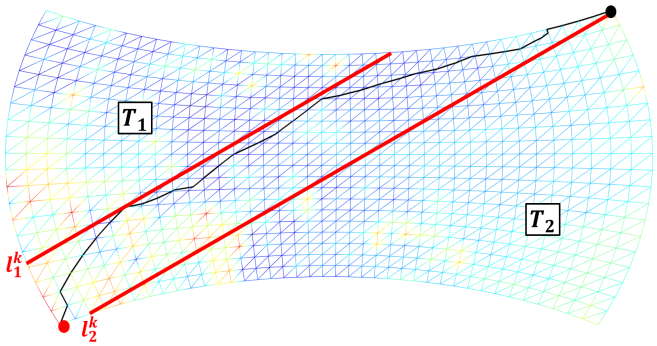

(b) $k = 1$. Producing the cable path γ_1 and identifying the decomposition lines l_1^k, l_2^k that enclose the cable path γ_1.

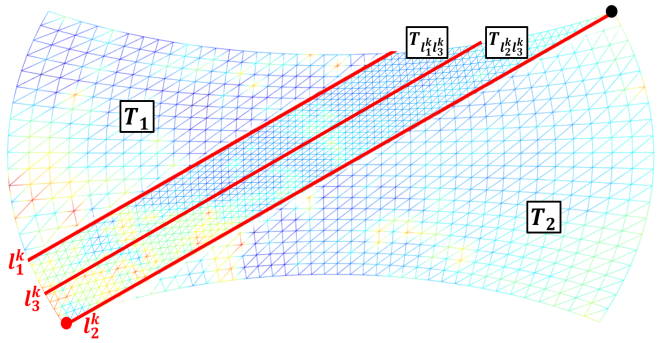

(c) $k = 2$. Increasing the resolution for area $T_{l_1^k l_2^k}$ between l_1^k and l_2^k, and dividing $T_{l_1^k l_2^k}$ into two sub-domains $T_{l_1^k l_3^k}$ and $T_{l_2^k l_3^k}$.

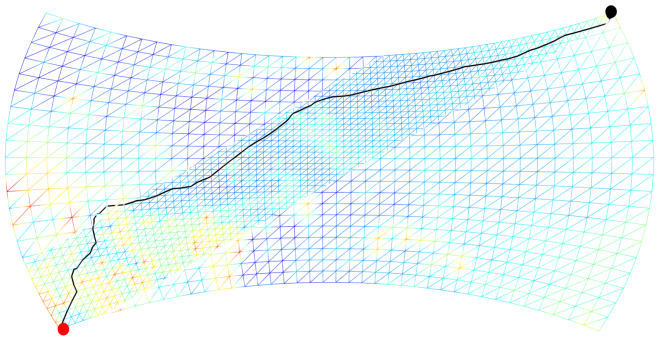

(d) $k = 2$. Producing the optimal cable path γ_2 under Fig. 10(c).

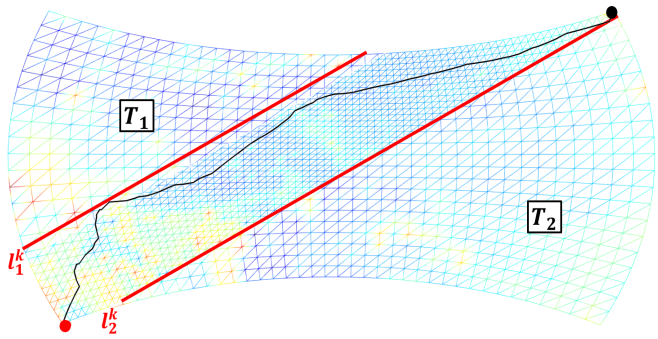

(e) $k = 3$. Identifying the decomposition lines l_1^k, l_2^k that enclose the cable path γ_2.

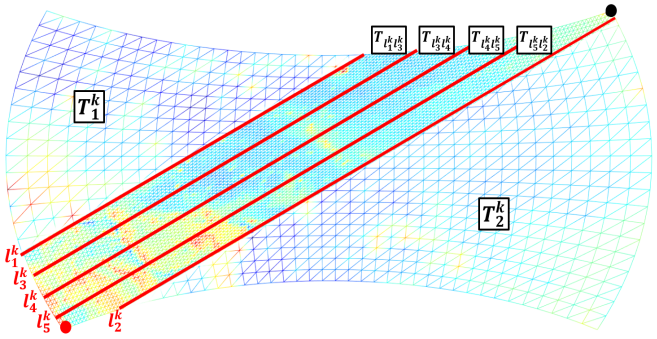

(f) $k = 3$. Increasing the resolution for area $T_{l_1^k l_2^k}$ between l_1^k and l_2^k, and dividing $T_{l_1^k l_2^k}$ into four sub-domains $T_{l_1^k l_3^k}$, $T_{l_3^k l_4^k}$, $T_{l_4^k l_5^k}$ and $T_{l_5^k l_2^k}$.

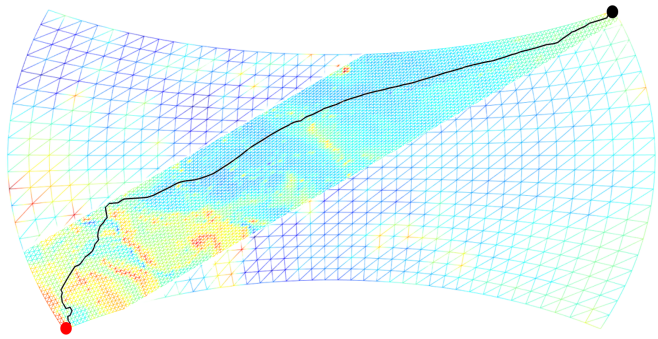

(g) $k = 3$. Producing the optimal cable path γ_3 under Fig. 10(f).

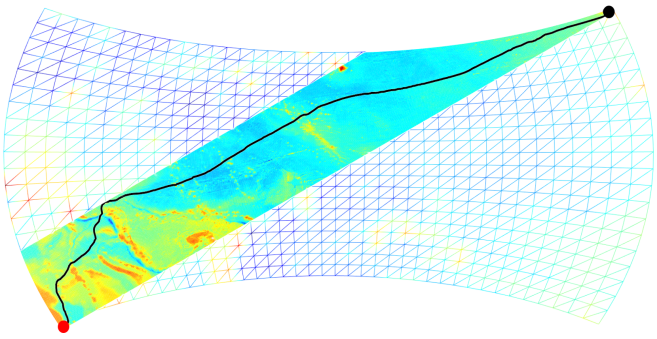

(h) $k = 7$. Final submarine cable path γ_7 for APFMM.

Fig. 10: 3D implementation process of APFMM viewed from the XOY plane.

our APFMM, where we always employ decomposition lines that are parallel to $\overrightarrow{AB}$. Such a comparative setup is designed to explore whether the domain decomposition method in our APFMM can better reduce the frequency of rollbacks during the parallelization process and enhance parallel efficiency. The comparison results are shown in Fig. 11 and Table V.

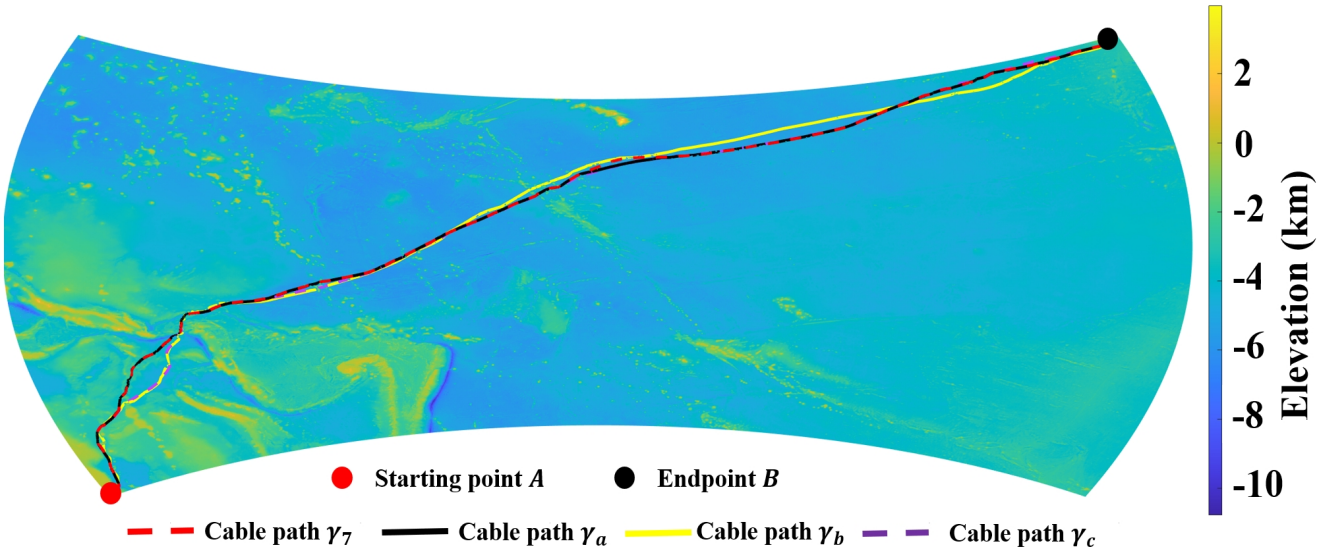

Fig. 11: Comparisons among 3D cable paths obtained by APFMM (γ_7), SFMM (γ_a), PFMM-I (γ_b), and PFMM-II (γ_c) on the XOY plane.

TABLE V: Numerical comparisons among cable paths obtained by APFMM (γ_7), SFMM (γ_a), PFMM-I (γ_b), and PFMM-II (γ_c).

Cable path	Running time (s)	*RF* ($\times 10^{-4}$)	Average distance between two adjacent grid points (km)	Number of grid points in T ($\times 10^6$)	Total length of cable path (km)	Total life-cycle cost ($\times 10^6$ \$)
γ_7 (APFMM)	4575	0.1201	0.0671	24.4673	14516.94	397.6001
γ_a (PFMM-I)	24541	5.979	0.0956	72.0324	14522.61	397.7590
γ_b (PFMM-II)	39946	11.78	0.0941	72.0324	14603.89	399.9521
γ_c (SFMM)	184923	NA	1.5231	8.2578	14584.75	399.3953

To assess the frequency of rollbacks and parallel efficiency among APFMM, PFMM-I, and PFMM-II, we employ a metric called

$$RF = \frac{\text{Total number of rollbacks}}{\text{Total number of grid points}}, \tag{12}$$

which is widely used in the existing literature to evaluate the parallel efficiency of parallel FMMs [17, 40]. The rollback procedure significantly impacts the algorithm's efficiency, as it necessitates both the re-computation of an accepted node and the visiting of all nodes within a sub-domain to identify the ones to rollback. Therefore, we use the *RF* value to accurately assess the parallel efficiency of parallel FMMs.

It is important to note that the processor we used in this paper has 14 cores and 20 threads, which means it can genuinely parallel process up to 20 threads at once. In simulations that require more than 20 threads, it is implemented through "time slicing," where the operating system quickly switches between multiple threads, allocating each a brief period of running time. This switching is so rapid that it appears as though the threads are running simultaneously. Such hardware limitations may only cause a slight delay in computation time, without affecting the accuracy of the *RF* metric calculations.

It can be seen in Fig. 11 that path γ_7 (red dashed line) obtained by APFMM is close to path γ_a (black solid line) of PFMM-I, while paths γ_b (yellow solid line) and γ_c (purple dashed line) obtained by PFMM-II and SFMM differ significantly from path γ_7 of APFMM. In more specific terms, the path γ_7, derived from our APFMM, presents the highest accuracy with the shortest average distance between the adjacent grid points being a mere 0.0671 km. Moreover, it boasts the quickest execution time of 4575 seconds, which saves about 81% of the time compared to PFMM-I and about 89% compared to PFMM-II, as illustrated in Table V. Conversely, path γ_c has the lowest accuracy with an average distance of 1.5231 km between adjacent grid points. It is noteworthy that although higher-resolution data is available in this case, SFMM struggles to load and process such data due to its completely serial nature. The precision of 1.5231 km average grid point distance is the highest achievable for SFMM, and the computation time has already reached 184923 seconds.

Table V shows that the frequency of rollbacks during the execution of APFMM is considerably lower compared to PFMM-I and PFMM-II. The *RF* value for APFMM is a mere 0.000012, significantly lower than the 0.00059 for PFMM-I and 0.00117 for PFMM-II. This improvement is attributed to the alignment of APFMM's sub-domain decomposition with $\overrightarrow{AB}$, which maintains consistency with the advancing direction of the path as closely as possible. This alignment effectively reduces the frequency of rollbacks and minimizes unnecessary communication overhead between adjacent sub-domains. Additionally, the incorporation of MRA significantly reduces the number of grid points that APFMM needs to process (by using lower resolutions in sub-domains that are far away from the cable path), further enhancing its efficiency compared to PFMM-I and PFMM-II. These factors collectively

result in a substantially shorter running time for APFMM. PFMM-II, in contrast, has a longer running time and a higher RF value than PFMM-I. This is due to PFMM-II's domain decomposition lines being perpendicular to $\overrightarrow{AB}$, which causes the path to persistently cross sub-domains during its advancement, thereby leading to an increase in rollbacks and a reduction in parallel efficiency.

In summary, the results from Table V demonstrate the significant advantages of our APFMM compared to PFMM-I, PFMM-II, and SFMM. Our proposed APFMM not only operates with very high parallel efficiency (as indicated by the very low *RF* values) within a remarkably short running time, but also successfully computes solutions with the smallest total length and total life-cycle cost. Specifically, the total life-cycle cost of the path solved by APFMM γ_7 is lower by 0.1589, 2.352, and 1.7952 million dollars compared to the paths of PFMM-I γ_a, PFMM-II γ_b, and SFMM γ_c, respectively. These advantages will greatly assist cable path planners in enhancing efficiency by providing high-quality path solutions as references and benchmarks.

It is important to highlight that although our experiments were performed in a simulated environment, the data used (as detailed in Section VI-B) was sourced from real-world datasets and was not artificially generated. This ensures that the data accurately reflects true oceanographic and other relevant factors, making our experimental results highly applicable to real-world scenarios. Additionally, these simulations showcase the effectiveness of our APFMM in handling ultra-long-distance and high-precision submarine cable path planning based on high-resolution data density. These require large-scale data processing, a novel aspect that previous research in the area has not addressed, representing a significant innovation in our study. Moreover, the paths designed using our APFMM algorithm can serve as valuable references and benchmarks for industrial planners involved in submarine cable path planning. Therefore, using APFMM in conjunction with data on existing cables, practitioners can analyze the risks and rationality of current submarine cable planning more effectively. This further underscores the practical importance and applicative potential of our study in the field.

VII. Conclusion

In this paper, we introduced a novel adaptive parallel FMM, namely APFMM, which for the first time integrates an adaptive DDM with a dynamic MRA. This combination offers a scalable methodology for planning high-precision, ultra-long-distance submarine cable routes over 14,000 kilometers. We demonstrated APFMM's superiority in submarine cable path planning compared to two other parallel FMMs and the traditional sequential FMM. Simulated results substantiated that APFMM overcomes the computational limitations of the sequential FMM with massive datasets and reduces running time by over 81% compared to traditional PFMMs, enabling efficient, automated long-distance submarine cable path planning. Moreover, considering that the current practice of submarine cable path design heavily relies on manual, expert-driven methods, which are not only time-consuming and labor-intensive but also often fail to consider many influencing factors simultaneously, the work presented in this paper serves as a reference and benchmark for cable path planners for optimal solutions given the data, fostering enhancements in future cable path planning endeavors.

However, it is important to note that although Table IV shows that increasing the number of sub-domains can yield higher precision and quality in path results (especially when dealing with high data resolution density or more design considerations under complex geographic conditions), it also introduces limitations and we should not indiscriminately pursue a greater number of sub-domains. An increasing number of sub-domains not only demands more from computational hardware, but also complicates inter-domain communication and potentially increases the frequency of rollbacks (as indicated by the higher *RF* value in Table IV), significantly reducing computational efficiency. This contradicts our initial objective of achieving highly efficient and automated long-distance, high-precision submarine cable path planning. Another limitation is associated with the practical challenge of acquiring more data, including higher resolution data and data needed by design considerations that we have not considered, e.g., sediment hardness and existing cables/pipelines. Therefore, future work will focus on optimizing the number of sub-domains relative to the target area size and computational capabilities, aiming to balance high-precision planning with computational efficiency. Additionally, we will explore and incorporate more design factors that influence the cost-effectiveness and reliability of submarine cables.

Acknowledgment

The authors would like to thank Prof. Uzi Vishkin for his participation and comments in a discussion on this study. We are also grateful to the anonymous reviewers for their thorough review and valuable insights, which have significantly enhanced our manuscript.

References

[1] J. Kim, "Submarine cables: the invisible fiber link enabling the Internet," 16 Jan., 2024 (accessed on 30 Jun., 2024). [Online]. Available: https://dgtlinfra.com/submarine-cables-fiber-link-internet/

[2] TeleGeography, "Submarine cable frequently asked questions," 2024 (accessed on 30 Jun., 2024). [Online]. Available: https://www2.telegeography.com/submarine-cable-faqs-frequently-asked-questions

[3] "Submarine cable systems market size," Global Market Insights Inc., 4 North Main Street, Selbyville, Delaware 19975, USA, Tech. Rep., Jun. 2024 (accessed on 30 Jun., 2024). [Online]. Available: https://www.gminsights.com/industry-analysis/submarine-cable-systems-market

[4] T. Blaubach, "Connecting Beijing's Global Infrastructure: The PEACE Cable in the Middle East and North Africa," 7 Mar., 2022 (accessed on 30 Jun., 2024). [Online]. Available: https://www.mei.edu/publications/connecting-beijings-global-infrastructure-peace-cable-middle-east-and-north-africa

[5] C. Mims, "Google, Amazon, Meta and Microsoft weave a fiber-optic web of power," 15 Jan., 2022 (accessed on 30 Jun., 2024). [Online]. Available: https://www.wsj.com/articles/google-amazon-meta-and-microsoft-weave-a-fiber-optic-web-of-power-11642222824

[6] X. Wang, Z. Wang, E. Tahchi, and M. Zukerman, "Submarine cable path planning based on weight selection of design considerations," *IEEE Access*, vol. 9, pp. 123 847–123 860, Aug. 2021.

[7] W. Qiu, "Submarine cables cut after Taiwan earthquake in Dec 2006," Mar. 2011 (accessed on 30 Jun., 2024). [Online]. Available: https://www.submarinenetworks.com/en/nv/news/cables-cut-after-taiwan-earthquake-2006

[8] X. Wang, Z. Wang, T. Wang, and M. Zukerman, "Designing cost-effective and reliable submarine communications cable path: Lessons from the Tonga volcano disaster," *IEEE Commun. Mag.*, vol. 61, no. 7, pp. 179–185, Feb. 2023.

[9] J. A. Sethian, "Fast marching methods," *SIAM Review*, vol. 41, no. 2, pp. 199–235, 1999.

[10] R. K. Mandava, K. Mrudul, and P. R. Vundavilli, "Dynamic motion planning algorithm for a biped robot using fast marching method hybridized with regression search," *Acta Polytech. Hung*, vol. 16, pp. 189–208, 2019.

[11] K. Mrudul, R. K. Mandava, and P. R. Vundavilli, "An efficient path planning algorithm for biped robot using fast marching method," *Procedia Comput. Sci.*, vol. 133, pp. 116–123, Jul. 2018.

[12] R. K. Mandava, M. Katla, and P. R. Vundavilli, "Application of hybrid fast marching method to determine the real-time path for the biped robot," *Intell. Serv. Robot.*, vol. 12, pp. 125–136, Nov. 2019.

[13] Z. Wang, Q. Wang, B. Moran, and M. Zukerman, "Optimal submarine cable path planning and trunk-and-branch tree network topology design," *IEEE/ACM Trans. Netw.*, vol. 28, no. 4, pp. 1562–1572, May 2020.

[14] T. Wang, Z. Wang, B. Moran, X. Wang, C. Guo, and M. Zukerman, "Latency-aware optimization of submarine communication cable systems with trunk-and-branch topologies," *J. Light. Technol.*, vol. 40, no. 17, pp. 5825–5841, Jun. 2022.

[15] T. Wang, Z. Wang, B. Moran, and M. Zukerman, "Submarine cable network design for regional connectivity," *IEEE/ACM Trans. Netw.*, vol. 30, no. 6, pp. 2480–2492, May 2022.

[16] Q. Wang, J. Guo, Z. Wang, E. Tahchi, X. Wang, B. Moran, and M. Zukerman, "Cost-effective path planning for submarine cable network extension," *IEEE Access*, vol. 7, pp. 61 883–61 895, May 2019.

[17] M. Breuß, E. Cristiani, P. Gwosdek, and O. Vogel, "An adaptive domain-decomposition technique for parallelization of the fast marching method," *Appl. Math. Comput.*, vol. 218, no. 1, pp. 32–44, Jun. 2011.

[18] G. Evans and M. Page, "The planning and surveying of submarine cable routes," in *Submarine Cables*. Brill Nijhoff, Jan. 2014, pp. 91–122.

[19] Makai Ocean Engineering, "Submarine cable services," 2015 (accessed on 30 Jun., 2024). [Online]. Available: https://www.makai.com/

[20] S. Neumayer, G. Zussman, R. Cohen, and E. Modiano, "Assessing the vulnerability of the fiber infrastructure to disasters," *IEEE/ACM Trans. Netw.*, vol. 19, no. 6, pp. 1610–1623, Apr. 2011.

[21] P. N. Tran and H. Saito, "Geographical route design of physical networks using earthquake risk information," *IEEE Commun. Mag.*, vol. 54, no. 7, pp. 131–137, Jul. 2016.

[22] M. Zhao, T. W. Chow, P. Tang, Z. Wang, J. Guo, and M. Zukerman, "Route selection for cabling considering cost minimization and earthquake survivability via a semi-supervised probabilistic model," *IEEE Trans. Ind. Inform.*, vol. 13, no. 2, pp. 502–511, Jul. 2016.

[23] G. Verikios, F. Janssen, A. Satish, and Y. Liu, "Spatial optimization for energy island location and cable routing considering offshore zoning," *Journal of Physics: Conference Series*, vol. 2767, no. 6, p. 062022, Jun. 2024.

[24] N. Makrakis, P. N. Psarropoulos, and Y. Tsompanakis, "GIS-based optimal route selection of submarine cables considering potential seismic fault zones," *Appl. Sci.*, vol. 13, no. 5, p. 2995, Feb. 2023.

[25] S. K. Routray, G. Sahin, J. R. F. da Rocha, and A. N. Pinto, "Deployment route length estimation in optical transport networks," *J. Light. Technol.*, to be published.

[26] Z. Zhao, J. Wang, G. Gao, H. Wang, and D. Wang, "Multi-objective optimization for submarine cable route planning based on the ant colony optimization algorithm," *Photonics*, vol. 10, no. 8, p. 896, Aug. 2023.

[27] D. Li, L. Wang, J. Cai, K. Ma, and T. Tan, "Research on terminal distance index-based multi-step ant colony optimization for mobile robot path planning," *IEEE Trans. Autom. Sci. Eng.*, vol. 20, no. 4, pp. 2321–2337, Oct. 2022.

[28] Z. Wang, Q. Wang, M. Zukerman, J. Guo, Y. Wang, G. Wang, J. Yang, and B. Moran, "Multiobjective path optimization for critical infrastructure links with consideration to seismic resilience," *Comput.-Aided Civ. Infrastruct. Eng.*, vol. 32, no. 10, pp. 836–855, Jul. 2017.

[29] C. Huang, Z. Ming, and H. Huang, "Drone stations-aided beyond-battery-lifetime flight planning for parcel delivery," *IEEE Trans. Autom. Sci. Eng.*, vol. 20, no. 4, pp. 2294–2304, Oct. 2022.

[30] Q. Wang, Z. Wang, J. Guo, E. Tahchi, X. Wang, B. Moran, and M. Zukerman, "Path planning of submarine cables," in *Proc. 21st International Conference on Transparent Optical Networks (ICTON)*, Angers, France, Jul. 2019.

[31] S. Blaise and B. Spinewine, "Efficient curvature-constrained least cost route optimization on parallel architectures," *Eng. Comput.*, pp. 1–17, Mar. 2021.

[32] P. Kotas, R. Croce, V. Poletti, V. Vondrak, and R. Krause, "A massive parallel fast marching method," in *Domain Decomposition Methods in Science and Engineering XXII*. Springer, 2016, pp. 311–318.

[33] M. Akian, S. Gaubert, and S. Liu, "A multilevel fast-marching method," in *Proc. 25th International Symposium on Mathematical Theory of Networks and Systems*

(MTNS), Bayreuth (DE), Germany, Sep. 2022.

[34] J. Xin, G. Xie, B. Yan, M. Shan, P. Li, and K. Gao, "Multimobile robot cooperative localization using ultra-wideband sensor and GPU acceleration," *IEEE Trans. Autom. Sci. Eng.*, vol. 19, no. 4, pp. 2699–2710, Oct. 2021.

[35] Y. Huang, "Improved fast iterative algorithm for Eikonal equation for GPU computing," *arXiv preprint arXiv:2106.15869*, 2021.

[36] J. Monsegny, J. Monsalve, K. León, M. Duarte, S. Becerra, W. Agudelo, and H. Arguello, "Fast marching method in seismic ray tracing on parallel GPU devices," in *Proc. Latin American High Performance Computing Conference (CARLA)*, Bucaramanga, Colombia, Sep. 2018, pp. 101–111.

[37] V. Dolean, P. Jolivet, and F. Nataf, *An introduction to domain decomposition methods: algorithms, theory, and parallel implementation*. Philadelphia, PA: Society for Industrial and Applied Mathematics, 2015.

[38] B. F. Smith, "Domain decomposition methods for partial differential equations," in *Parallel Numerical Algorithms*. Springer, 1997, pp. 225–243.

[39] X. Cai, "Overlapping domain decomposition methods," in *Advanced Topics in Computational Partial Differential Equations: Numerical Methods and Diffpack Programming*. Springer, 2003, pp. 57–95.

[40] M. Herrmann, "A domain decomposition parallelization of the fast marching method," *Center for Turbulence Research Annual Research Briefs*, Jan. 2003.

[41] G. Diamantopoulos, J. Weinbub, A. Hössinger, and S. Selberherr, "Evaluation of the shared-memory parallel fast marching method for re-distancing problems," in *Proc. 17th International Conference on Computational Science and its Applications (ICCSA)*, Trieste, Italy, Jul. 2017.

[42] A. Rosenfeld, *Multiresolution image processing and analysis*. Springer Science & Business Media, 2013, vol. 12.

[43] H. Wu, Z. Zhao, and Z. Wang, "META-Unet: Multi-scale efficient transformer attention Unet for fast and high-accuracy polyp segmentation," *IEEE Trans. Autom. Sci. Eng.*, vol. 21, no. 3, pp. 4117–4128, Jul. 2024.

[44] X. Wang, G. Cheng, Z. Wang, and M. Zukerman, "A research on submarine cable path planning," in *Proc. 8th Symposium on Novel Photoelectronic Detection Technology and Applications*, Mar. 2022, pp. 512–519.

[45] M. Zukerman, Z. Wang, Q. Wang, W. Moran, X. Wang, E. Tahchi, and F. C. Leung, "Infrastructure link path arrangement determination method and system," Jan. 18 2022, US Patent 11,228,523.

[46] G. Diamantopoulos, A. Hössinger, S. Selberherr, and J. Weinbub, "A shared memory parallel multi-mesh fast marching method for re-distancing," *Adv. Comput. Math.*, vol. 45, pp. 2029–2045, Apr. 2019.

[47] J. Weinbub and A. Hössinger, "Shared-memory parallelization of the fast marching method using an overlapping domain-decomposition approach," in *Proc. 24th High Performance Computing Symposium (HPC'16)*, Pasadena, California, Apr. 2016.

[48] M. Quell, G. Diamantopoulos, A. Hössinger, and J. Weinbub, "Shared-memory block-based fast marching method for hierarchical meshes," *J. Comput. Appl. Math.*, vol. 392, p. 113488, Aug. 2021.

[49] ITU, "Maximising availability of international connectivity in developing countries: Strategies to ensure global digital inclusion," Dec. 2016 (accessed on 30 Jun., 2024). [Online]. Available: http://handle.itu.int/11.1002/pub/80f5eade-en

[50] K. Eriksson, D. Estep, and C. Johnson, *Applied mathematics: Body and soul: Volume 1: Derivatives and geometry in IR3*. Springer Science & Business Media, 2013.

[51] D. Burago, Y. Burago, and S. Ivanov, *A course in metric geometry*. American Mathematical Society, 2022, vol. 33.

[52] J. A. Sethian *et al.*, *Level set methods and fast marching methods*. Cambridge Cambridge UP, 1999, vol. 98, no. 2.

[53] R. Kimmel and J. A. Sethian, "Optimal algorithm for shape from shading and path planning," *J. Math. Imaging Vis.*, vol. 14, pp. 237–244, 2001.

[54] R. Kimmel and J. A. Sethian, "Computing geodesic paths on manifolds," in *Proc. Natl. Acad. Sci.*, vol. 95, Jul. 1998, pp. 8431–8435.

[55] K.-H. Hoffmann and J. Zou, "Parallel efficiency of domain decomposition methods," *Parallel Comput.*, vol. 19, no. 12, pp. 1375–1391, Dec. 1993.

[56] E. Cristiani and M. Falcone, "A characteristics driven fast marching method for the Eikonal equation," in *Proc. 7th European Conference on Numerical Mathematics and Advanced Applications (ENUMATH)*, Graz, Austria, Sep. 2007, pp. 695–702.

[57] ICPC, "Submarine cables cut after Taiwan earthquake in Dec 2006," Aug. 2023 (accessed on 30 Jun., 2024). [Online]. Available: https://www.iscpc.org/publications/recommendations/

[58] G. W. McDonald, N. J. Smith, J.-h. Kim, S. J. Cronin, and J. N. Proctor, "The spatial and temporal 'cost' of volcanic eruptions: assessing economic impact, business inoperability, and spatial distribution of risk in the Auckland region, New Zealand," *Bulletin of Volcanology*, vol. 79, pp. 1–13, Jun. 2017.

[59] L. Carter, *Submarine cables and the oceans: connecting the world*. UNEP/Earthprint, 2009, no. 31.

Xinyu Wang received his B.Eng. degree in Electronic Science and Technology from Zhejiang University in Hangzhou, and his M.Sc. degree in Electronic Information Engineering and Ph.D. degree in Electrical Engineering from City University of Hong Kong, Hong Kong SAR, China. He is currently a postdoctoral researcher in the Center for Intelligent Multidimensional Data Analysis, Hong Kong SAR, China. His research focuses on path planning and resource allocation within telecommunication networks.

Zengfu Wang received the B.Sc. degree in applied mathematics, the M.Sc. degree in control theory and control engineering, and the Ph.D. degree in control science and engineering from Northwestern Polytechnical University, Xi'an, China, in 2005, 2008, and 2013, respectively. From 2014 to 2017, he was a Lecturer at Northwestern Polytechnical University, where he is currently an Associate Professor. From 2014 to 2015, he was a Postdoctoral Research Fellow at the Department of Electronic Engineering, City University of Hong Kong, Hong Kong. From 2019 to 2020, he was a Visiting Researcher with the Faculty of Electrical Engineering, Mathematics and Computer Science, Delft University of Technology, Delft, The Netherlands. His research interests include path planning, discrete optimization, and information fusion.

Moshe Zukerman (M'87-SM'91-F'07-LF'20) received the B.Sc. degree in industrial engineering and management, the M.Sc. degree in operations research from the Technion–Israel Institute of Technology, Haifa, Israel, and the Ph.D. degree in engineering from University of California, Los Angeles, in 1985. He was an independent consultant with the IRI Corporation and a Postdoctoral Fellow with the University of California, Los Angeles, in 1985–1986. In 1986–1997, he was with Telstra Research Laboratories (TRL), first as a Research Engineer and, in 1988–1997, as a Project Leader. He also taught and supervised graduate students at Monash University in 1990–2001. During 1997–2008, he was with The University of Melbourne, Victoria, Australia. In 2008 he joined City University of Hong Kong as a Chair Professor of Information Engineering, and a team leader. From December 2020, he also serves as Acting Chief Information Officer of CityU. He has over 300 publications in scientific journals and conference proceedings. He has served on various editorial boards such as COMPUTER NETWORKS, the IEEE Communications Magazine, the IEEE JOURNAL OF SELECTED AREAS IN COMMUNICATIONS, the IEEE/ACM TRANSACTIONS ON NETWORKING, and Computer Communications.